Full–length paper

Practical considerations on the determination of the accuracy of the lattice parameters measurements from digital recorded diffractograms

Johannes Biskupek* and Ute Kaiser[1]

Friedrich-Schiller-University, Institute of Solid State Physics, Helmholtzweg 5, D-07743 Jena, Germany
[1]Present address: Technical University Ilmenau, Centre of Micro- and Nanotechnologies, Kirchoffstrasse 1, D-98693 Ilmenau, Germany
*To whom correspondence should be addressed. E-mail: biskupek@pinet.uni-jena.de

Abstract   The influence of magnification and defocus on the precision $\Delta d/d$ of lattice parameter measurements have been studied by evaluating the diffraction vector length and the signal-to-noise ratio (SNR) of the diffraction peaks in diffractograms calculated by fast Fourier transformation (FFT) of digitally recorded images. Examples are perfect crystals (Si and SiC) and defective crystals (two- and three-dimensional defects within SiC). It is shown that the precision is independent of the diffuseness of the FFT reflections caused by defocus changes or by two-dimensional defects. For the case of a perfect and/or a defective but unstrained crystal, the precision $\Delta d/d$ is linearly dependent on the diffraction vector length. For optimal conditions, the highest precision is 0.002. For a defective crystal containing precipitates (nanocrystals), it was found for both the matrix and the nanocrystals that the precision of the measurement is determined by the contribution of strain value $(\Delta d/d)_{strain}$ of the defective crystal and accuracy $\Delta d/d$ for the perfect matrix crystal.

Introduction

Devices fabricated by nanotechnology possess important structure on the nanometre scale. Properties of materials are modified in comparison to the bulk if they are manipulated at this scale. Therefore, it is essential that they be characterized at close to the atomic level. An important property of a nano-object and its matrix is their lattice parameters and it is essential to know the precision with which they have been determined. Very high accuracy of lattice parameters (better than 10^{-6}) can be obtained by X-ray measurements (e.g. [1]); however, this technique averages over a large specimen volume. Using the most recent techniques developed in convergent-beam electron diffraction, lattice parameters from a relatively small specimen area can be obtained with an accuracy up to 10^{-5} (e.g. [2–4]); however, a perfect crystal and a transmission electron microscope (TEM) specimen with a thickness of ~200 nm are required. For structures small in all three dimensions (some nanometres

in size) and for a defective matrix crystal, the only method is the determination of the lattice parameters from high-resolution (HR) TEM images. There are basically two equivalent approaches: the direct space (image) and the reciprocal space (corresponding diffractogram) analyses. However, direct space analysis is inconvenient practically if the internal calibration standard of the TEM is used, as this requires images to be recorded under identical conditions of beam size, eucentric height and defocus as those at which the TEM was calibrated. An alternative direct space method is calibration with a perfect standard sample or recalibrating recorded images using known lattice plane distances present in the HRTEM images. The estimated error is reported to be 0.5% [5,6] for the case of a perfect crystal.

There are a number of excellent reports on the accuracy of lattice parameter determination based on reciprocal space analysis measuring diffraction spot positions with subpixel accuracy in the Fourier transform patterns (FT)

(diffractograms) of digital recorded HRTEM images (filtered fast FT (FFT) is used to avoid streaking of reflections) [5,7–17]. For the case of a perfect matrix, the effect on the precision of the image size was investigated and this was shown to vary from 0.0007 nm ($\Delta d/d = 0.2\%$) to 0.035 nm ($\Delta d/d = 5\%$) (for 256×256 and 32×32 pixels, respectively) [7,8].

Most published investigations concentrate on the strain analysis of nanostructures. Rosenauer [9,10] and Hÿtch [11,12] developed software packages (DALI and NCEM phase-extension package) and detected and visualized strain in nanolayers to an accuracy of 0.003 nm ($\Delta d/d = 0.01$). Precise analyses of nanocrystal plane spacing revealed a dependence of lattice parameter on crystallite size and the existence of 'magic sizes' for Pb nanocrystals [13], while small Pd/Au nanocrystals were shown to have larger d-spacings than bulk material [5,14,18]. Image simulation on the basis of experimental images of different crystal types of nano-clusters were performed to avoid image misinterpretations (lattice fringes may not simply correspond to real planes in of the crystal structure), which can be caused by the change in space group and nanocrystal orientation [5,15–17].

A method combining reciprocal- and direct-space infor-mation was presented by Qin and Fraundorf [6]. The com-plete set of lattice parameters including space group has been determined from HRTEM images of WC_{1-x} nanocrystals up to the precision of 0.001 nm ($\Delta d/d = 0.005$). It was stated that the influence of the defocus near Scherzer-defocus might not affect the accuracy measured with the reciprocal space method [8]. However, other workers using the direct space method found small changes of the defocus led to variations in width measurements of 1 nm diameter nano-tubes of $\sim 5\%$ [19].

The present paper is based on the reciprocal space approach introduced by de Ruijter [7,8]. We discuss typical practical questions of the method, which, to the best of our knowledge, have not been addressed so far, such as:

(i) Which is the optimum magnification for the HRTEM images?
(ii) Does the signal-to-noise ratio (SNR) of the diffraction peaks vary with the blur of the FFT reflections caused by the defocus (defined as defocus noise) or with the blur of the FFT reflections caused by two- (2-D) and three-dimensional (3-D) defects? Two-dimensional defects are defects that are extended in two dimensions, such as interfaces and stacking-faults; 3-D defects are extended in all three dimensions, such as precipitates (nanocrys-tals) inside a matrix.
(iii) For the case of a 3-D defect in a matrix, how can the strain value of a matrix crystal and of the embedded nanocrystal inside the matrix be determined and how does this affect the accuracy of the lattice parameter measurements and what is the resulting accuracy?

These questions for the defective SiC will be considered using perfect SiC as a calibration reference.

Methods

Defective, precipitate-rich 4H-SiC and 6H-SiC were created by implantation with 2×10^{16} cm^{-2} 250 keV Ge$^+$ ions (into 4H-SiC) and 2×10^{16} cm^{-2} 400 keV Er$^+$ ions (into 6H-SiC) at 700°C, followed by annealing at 1600°C under 0.2 bar Ar atmosphere (for more details see [20–23]). Cross-sectional samples of perfect Si and perfect 4H-SiC and of defective 4H-SiC were prepared for TEM using mechanical polishing, dimpling and low-angle Ar-ion milling. Microscopy was carried out on a JEOL JEM3010 TEM (LaB$_6$ cathode, reso-lution 0.21 nm, information limit 0.17 nm). Digital HRTEM images were recorded with a Gatan Multiscan CCD camera MSC794 (1024×1024 pixels, pixel size 24×24 μm, gain corrected and anti-blooming enabled).

The image processing software Gatan Digital Micrograph 3.x (DM3) [24] was used. A DM3-script was used to auto-mate the FFT calculation and measurements of the d-values of the reflections were made with bilinear interpolation for subpixel detection [8].

Gross image distortions caused by condenser and objective lens astigmatism were minimized by careful application of standard alignment procedures. Displacement fields in HRTEM images of a perfect Si crystal due to fine objective lens distortions were determined with the DALI package [9] to be $<0.1\%$ for the magnifications used. This value includes also any possible distortion due to the CCD-chip of the camera, although these for the particular model of CCD camera used have been shown to be negligible [25,26].

To determine the accuracy of lattice parameters meas-urements for the case of a perfect crystal, two effects have been studied: the influence of image size (magnification) and the influence of defocus noise. For the first case, FFT patterns of HRTEM images of Si viewed along <110> were evaluated. The d-value of the $\bar{1}11$-reflection was calibrated (d$_{\bar{1}11}$ = 0.3136 nm (room temperature) [27]). The d-values of the $\bar{1}1\bar{1}$-, $\bar{2}20$- and 002-reflection were then measured and compared with the tabulated values of d$_{\bar{1}1\bar{1}}$ = 0.3136 nm, d$_{\bar{2}20}$ = 0.1920 nm, d_{002} = 0.2715 nm (Figs 1a and 1b). The results were averaged over 20 images from the same sample region (with the same orientation and thickness) for each magnification step (300 000, 400 000, 600 000 and 800 000, which correspond to defined numbers of recorded lattice planes in the HRTEM images). The standard deviation of the mean value is taken as an estimate of the error of the lattice spacing. To study the influence of defocus noise, [110] HRTEM images of perfect Si and [11$\bar{2}$0] HRTEM images of perfect 4H-SiC were taken and their FFTs were evaluated. For the case of 4H-SiC (Figs 1c and 1d), the 0004 reflection was calibrated (d_{0004} = 0.2521 nm (room temperature) [1]) and then the 1$\bar{1}$00 reflection was measured and compared with the tabulated value (d$_{1\bar{1}00}$ = 0.2668 nm).

The defocus was changed in steps of -5 nm, starting with near Scherzer-defocus (Scherzer focus for JEM3010 is at -64 nm) and ending at -159 nm underfocus. The results were averaged over 20 FFT patterns obtained from one
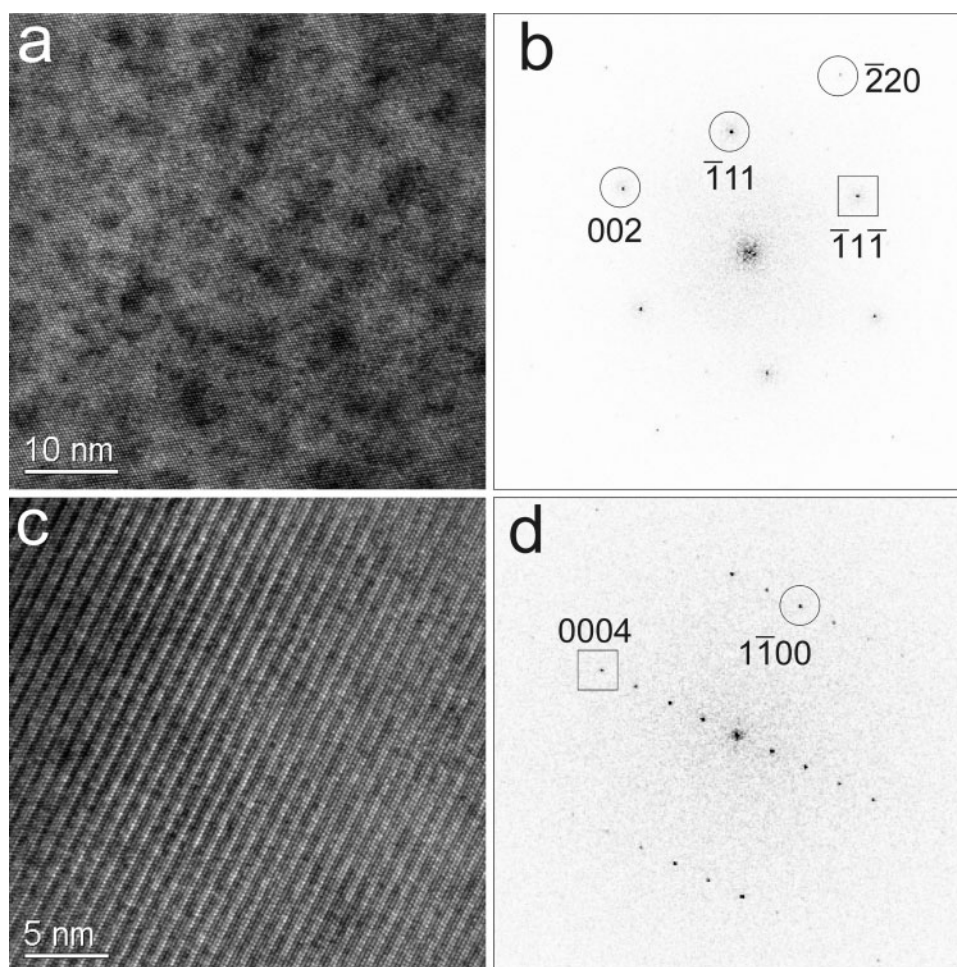
Fig. 1 HRTEM images (a, c) of Si [110] and 4H-SiC [11$\bar{2}$0], respectively, and the corresponding FFT patterns (b, d). The reflections marked by the squares were used for calibration of the images. The encircled reflections were measured and compared with the tabulated values.

defocus series. To measure the changes in the spot positions of the FFT patterns accurately, a SNR was defined as follows. A symmetric area of 18 nearest pixels around the central pixel of maximum intensity of a reflection spot was analysed. The deviation of intensity within this area was defined as noise. The SNR has been defined as

$$\text{SNR} = \frac{\text{intensity of central pixel of reflection}}{\text{deviation of intensity}}$$

The SNRs of the $\bar{1}$11 (Si) and 0004 (4H-SiC) reflections have been examined.

HRTEM images of nanocrystals created after Ge^+ (Er^+) ion implantation in 4H-SiC (6H-SiC) were obtained near Scherzer defocus at a magnification of 400 000. The FFT patterns were calculated from the whole image (1024 × 1024 pixels) and from parts of the image (512 × 512 or 256 × 256 pixels). The FFTs were calibrated with the 0004 reflection (0006 for the case of 6H-SiC, $d_{\text{SiC-0006}} = 0.2520$ nm) obtained from an undistorted matrix part in the same HRTEM image and compared with the 1$\bar{1}$00 reflection in the distorted part (around the defect). The difference between the measured and the tabulated 1$\bar{1}$00-reflections was treated as a measure

for the accuracy of the matrix and nanocrystals lattice parameters and allows the determination of the strain value. To visualize the strain and defects, local changes of selected FFT-reflection have been measured using the plug-in 'NCEM phase-extension package' for Digital Micrograph [11].

For HRTEM image simulation, the Java version of the Electron Microscopy Simulation package from P. Stadelman [28,29] was used. The simulation parameters were 300 kV, $C_S = 1.4$ mm, focus spread 50 Å, beam convergence 0.5 mrad, Debye–Waller factor 1.0 Å^2. Different SNR values have been realized artificially by applying noise by a Gaussian speckle-filter to calculated 4H-SiC HRTEM images.

Results

Limitations of the accuracy of the lattice parameter measurements for the case of perfect Si and perfect 4H-SiC

The influence of the diffraction vector length L^{-1}. In Figure 2, HRTEM images of Si [110] recorded at different magnifications are presented together with the corresponding
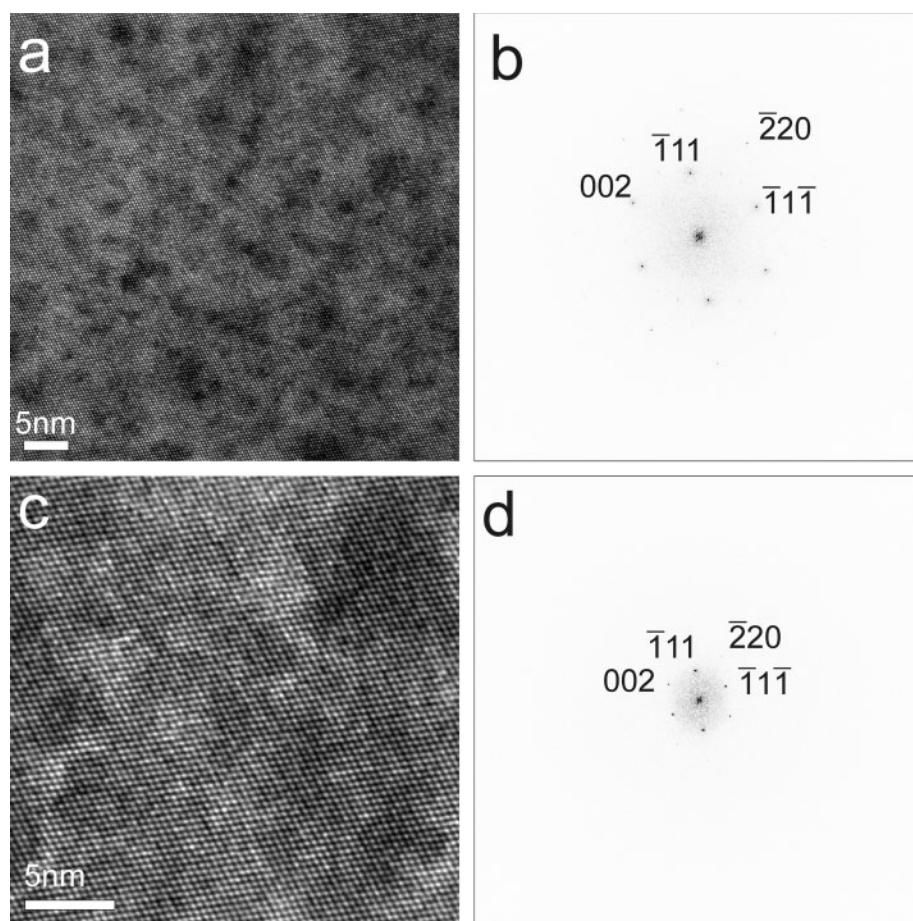
Fig. 2 [110] HRTEM image of Si recorded at a magnification of ×400 000 (a) and the calculated FFT pattern (b). HRTEM image of Si recorded at a magnification of ×800 000 (c) and the corresponding FFT pattern (d).

diffractograms. It is obvious that the lengths of the diffraction vectors in reciprocal nanometres per pixel are larger for the larger number of lattice planes and the error for the corresponding interplane distance is lower. When plotting $\Delta d/d$ over the value L^{-1} in pixels^{-1} for different diffraction vectors (L here is the distance between the FFT reflection and the origin in the calculated FFT pattern in pixels), the results were fitted by a linear approximation, assuming a detection error of 1 pixel around a reflection spot, as

$$\Delta d/d = A \cdot L^{-1} + B \qquad (1)$$

with $A = 1.02 \pm 0.14$ and $B = -0.0024 \pm 0.0015$ (see the solid line in Fig. 3). As A is close to 1.0 and B is close to zero, a good estimate of the accuracy can be obtained by simply setting $\Delta d/d$ equal to L^{-1} (dotted line in Fig. 3), which is a good estimate for the practical cases of d-values between 0.2 and 0.4 nm. The dependence on L implies that the relative precision $\Delta d/d$ ranges from 0.0015 to 0.01 depending on magnification and plane spacing. To get the highest accuracy in lattice parameters measurements (which for the JEM3010 is approximately 0.002), HRTEM images should be recorded at lower magnification. The longest $\boldsymbol{g}$-vectors for each given magnification should be examined. Equation 1 is
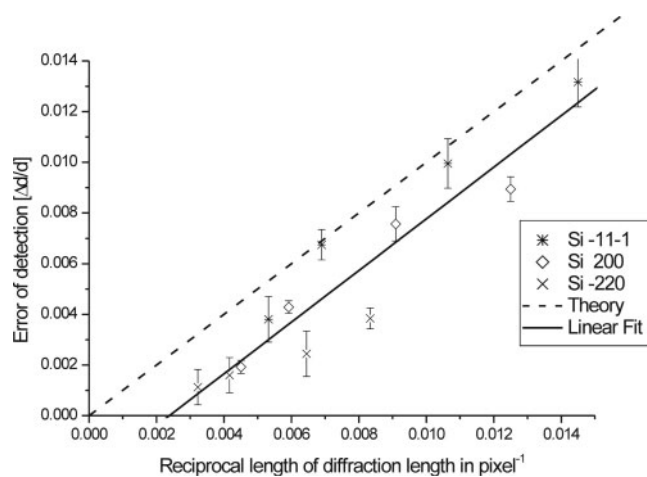
Fig. 3 Accuracy of lattice parameters $\Delta d/d$ as a function of L^{-1} (in pixel^{-1}). The fitted accuracy function (solid line) and the theoretical function (dotted line) are shown. Each data point of a reflection corresponds to another magnification.

also valid if only a part of the image is evaluated; however, a reduction in the number of pixels in the image will reduce the precision with which spots can be located in a diffractogram assuming that both partial and whole images
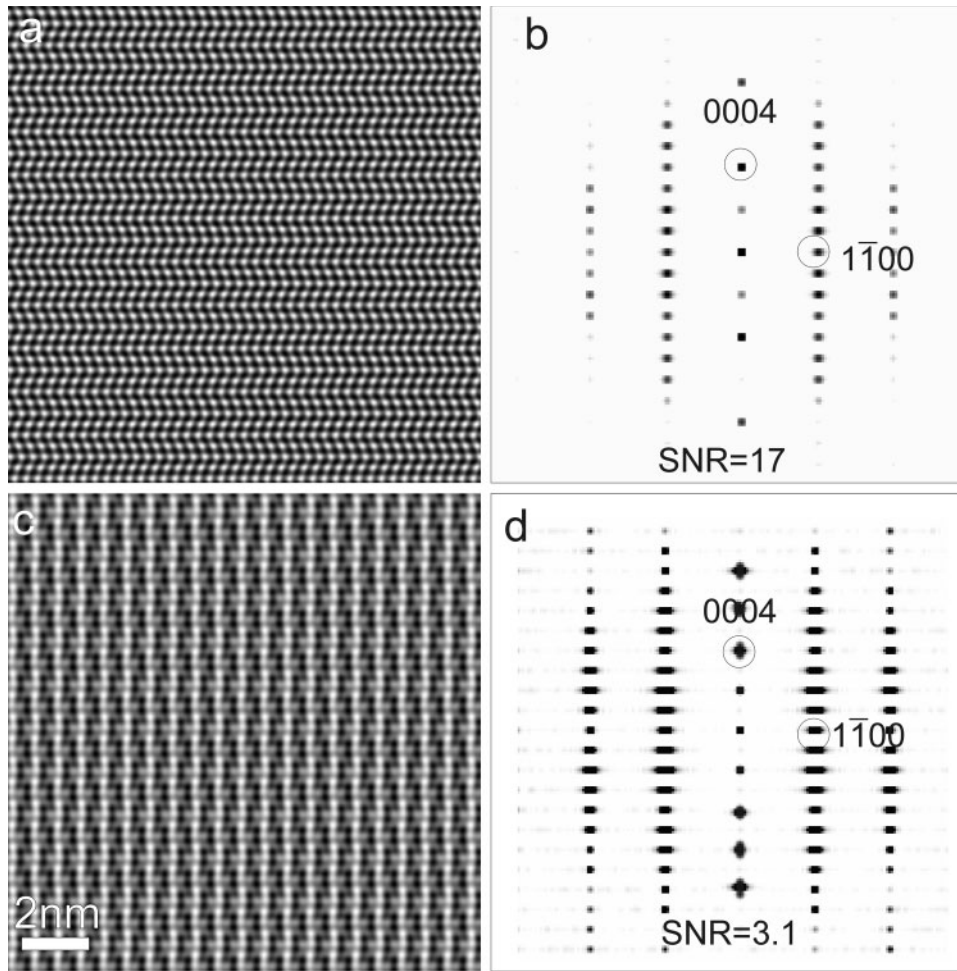
Fig. 4 Simulated HRTEM images of ($11\bar{2}0$) 4H-SiC (7 nm thickness) (a) at Scherzerfocus (-64 nm) with the corresponding diffractrogram (b). (c) HRTEM image at -360 nm underfocus with the corresponding diffractrogram (d). The SNRs for the 0004 reflections are indicated. The high underfocus leads not only to a blurred HRTEM image but also to a decrease in the SNR ratio of the FFT reflection.

come from perfect or uniformly strained crystals. Taking points mentioned into account, advised magnifications for best precision are $\times 300\,000$–$400\,000$.

The influence of defocus. If a crystal is imaged in high resolution far from Scherzer defocus, the image increases its diffuseness and the original structure of the lattice planes can no longer be recognized (compare Figs 4a and 4c, where simulations are shown at -64 nm defocus (Scherzer defocus conditions) and -360 nm, respectively). The corresponding Fourier transforms are more similar (compare Figs 4b and 4d); however, it can be easily seen that reflections in Fig. 4d are noisier than those in Fig 4b (most pronounced for 0004 and $1\bar{1}00$ reflections). As the experimental results of both 4H-SiC and Si were similar, only the data of the SNR for the 0004 reflection of 4H-SiC (solid line) are presented in Fig. 5a. As a consequence of the considerations above (see the section 'The influence of the diffraction vector length L^{-1}') an image size of 1024×1024 pixels and a magnification of $\times 400\,000$ was chosen. It can be seen from the figure that the SNR periodically decreases with

increasing negative defocus. For the first two oscillations, the period corresponds well with those of the oscillations of the square of the phase-contrast transfer function P (dotted line in Fig. 5a).

$$P = -\sin\left(\frac{\pi}{2}C_s\lambda^3 k^4 + \pi\Delta f\lambda k^2\right) \quad (2)$$

where C_S (spherical aberration) $= 1.4$ mm, λ (relativistic wavelength of the electrons) $= 0.00197$ nm, k (spatial frequency of $0004_{4H\text{-}SiC}$) $= 0.397$ nm^{-1} and Δf is the defocus. The third period of the experimental and theoretical curves does not coincide. The reasons for this may be non-equidistant defocus steps or small shifts in the position of frequency minima in P as a function of defocus caused by the damping function, which is not included in eq. (2) [30]. Figure 5b shows the detection error $\Delta d/d$ as a function of the SNR for both the experimental results and the simulations. The error increases only for SNRs ratios lower than 10. As those high SNRs have no practical relevance (see the SNRs of the images in Fig. 4), Fig. 5b demonstrates that the defocus
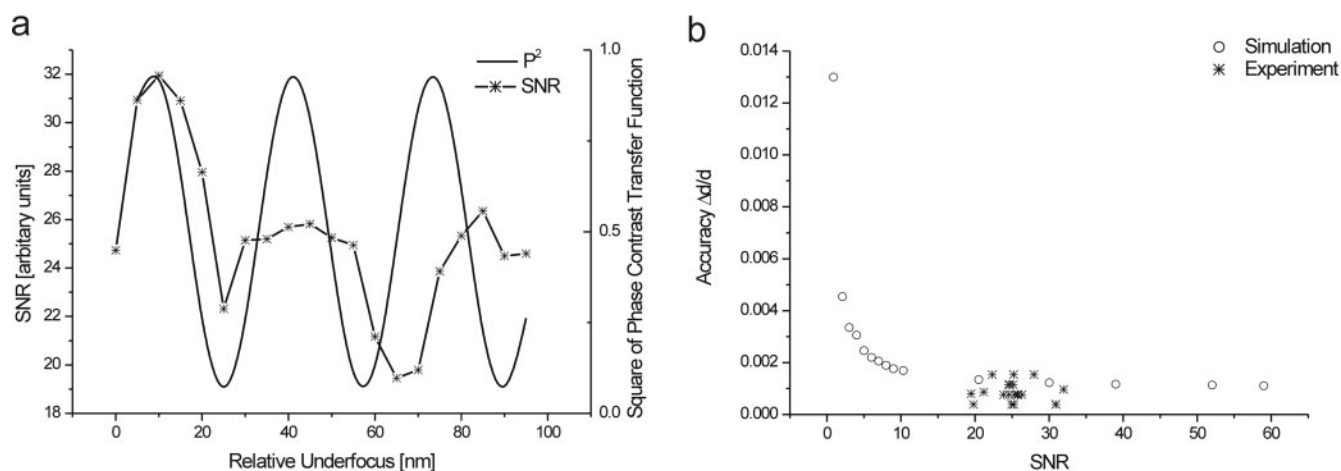
Fig. 5 (a) Measured SNR of the 0004 reflection of 4H-SiC as a function of the defocus (solid line) for diffractograms (size 1024×1024 pixels) calculated from experimental HRTEM images taken at a magnification of $\times 400\,000$. The SNR oscillates and slowly decreases with higher negative defocus. The defocus series were obtained from 0 nm (normalized from a subjective best chosen Scherzerfocus of -64 nm) to 100 nm underfocus. The dotted curve shows the dependence of the square of the phase-contrast transfer function (P) for the 0004-SiC reflection. (b) Accuracy $\Delta d/d$ for the $1\bar{1}00$ SiC reflection as a function of the SNR from experimental and calculated images. Calculated 4H-SiC HRTEM images have been overlaid with Gaussian blurring filters resulting in different SNRs (see 'Methods').
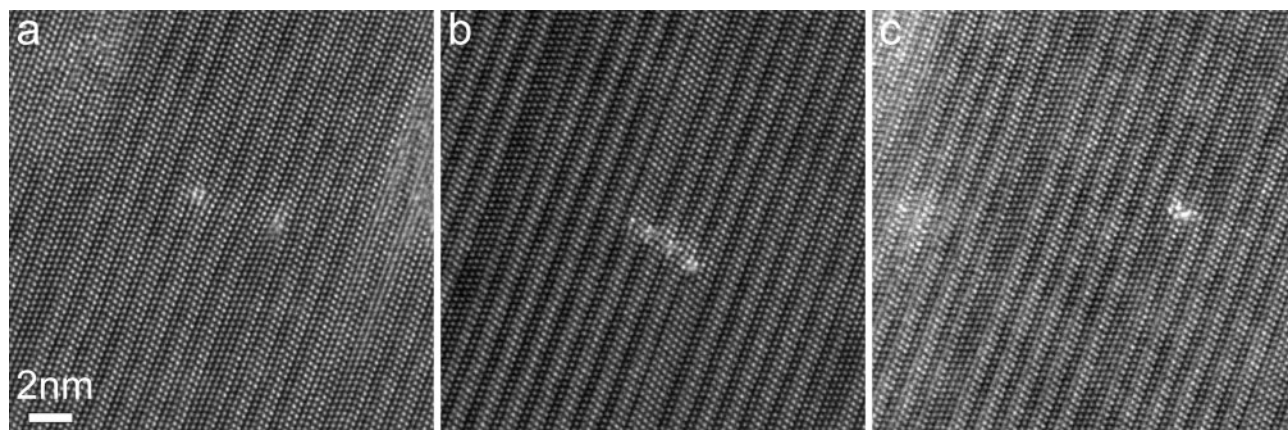
Fig. 6 The $(11\bar{2}0)$ HRTEM images of 2-D defects created after Ge implantation into SiC.

in practice does not affect the accuracy of lattice parameter measurements, confirming the assumptions made in earlier work [7].

Limitations of the accuracy of the lattice parameters measurements for the case of defective 4H-SiC

Two-dimensional defects inside a crystalline matrix. The $(11\bar{2}0)$HRTEM images of ion-implanted SiC show 2-D defects as wide interstitial loops (see the HRTEM images in Fig. 6) where foreign atoms agglomerate at their edges, as was shown earlier by HAADF-STEM imaging [31]. Here we investigate how 2-D defects influence the SNR and d-value of $1\bar{1}00$ reflections in the whole image (1024×1024 pixels) and in two smaller parts (512×512 and 256×256 pixels). (The defect was kept in the centre of the image at all times.) For all defects in Fig. 6, the $d_{1\bar{1}00}$ reflection differs in the order of 1%, indicating strain. However, it was found that

the SNR is not significantly influenced by the lattice parameter strain nor by the image size (the SNR varies between 15 and 17 for the different image sizes). Table 1 shows the accuracy and d-values for the $1\bar{1}00$ reflection. For the smallest image part (256×256 pixels) the measurement accuracy was estimated to be $\Delta d/d = 0.005$ from the number of lattice planes in the field of view using eq. (1). This value is much less than $(\Delta d/d)_{\text{strain}}$ calculated from the local change in plane spacing relative to the perfect crystal $(d - d_0)/d = 0.01$ of the defective (strained) image.

Three-dimensional defects inside a crystalline matrix. Evaluation of the accuracy of lattice parameter measurements in the presence of precipitates embedded in a crystalline matrix (nanocrystals formed in hexagonal SiC after Er and Ge implantation, the nanocrystal width is about a quarter of the full image width (matrix with nanocrystals)) is essential to determine the accuracy of the lattice parameters measurements both for the matrix and for the precipitate.

Table 1. The *d*-values and SNR of the $1\bar{1}00$ -reflections for different FFT-box sizes and defects shown in Figs 6a–c. The strain has been calculated by $(d - d_0)/d$

Image source	FFT box 1024×1024 (whole image)		FFT box 512×512 (around the defect)		FFT box 256×256 (around the defect)	
	d-value (nm)	Strain	*d*-value (nm)	Strain	*d*-value (nm)	Strain
Fig. 6a	0.2669	0.0004	0.2654	−0.0053	0.2601	−0.0257
Fig. 6b	0.2667	−0.0004	0.2668	0	0.2678	0.0037
Fig. 6c	0.2670	0.0007	0.2689	0.0078	0.2729	0.0223

Table 2. Measured *d*-values of nanocrystal and matrix as well as the calculated strain for the different parts of the image shown in Fig. 7. Table values are $d_{SiC\ 1-100} = 0.2668$ nm, $d_{GeSi\ 1-100} = 0.3436$ nm (for $Ge_{0.8}Si_{0.2}$). The strain has been calculated by $(d-d_0)/d$

| Reflection	FFT box 1024×1024 (whole image)		FFT box 512×512 (around the nanocrystal)		FFT box 256×256 (around the nanocrystal)		FFT box 256×256 (undistorted area)	
	d-value (nm)	Strain	*d*-value (nm)	Strain	*d*-value (nm)	Strain	*d*-value (nm)	Strain
$1\bar{1}00_{SiC}$	0.2670	+0.0007	0.2662	−0.002	0.2654	−0.005	0.2666	−0.0008
$1\bar{1}00_{GeSi}$	0.3326	−0.033	0.3316	−0.036	0.3313	−0.037		
$01\bar{1}0_{GeSi}$	0.3319	−0.035	0.3311	−0.038	0.3313	−0.037		
$\bar{1}010_{GeSi}$	0.3307	−0.039	0.3297	−0.042	0.3267	−0.051		
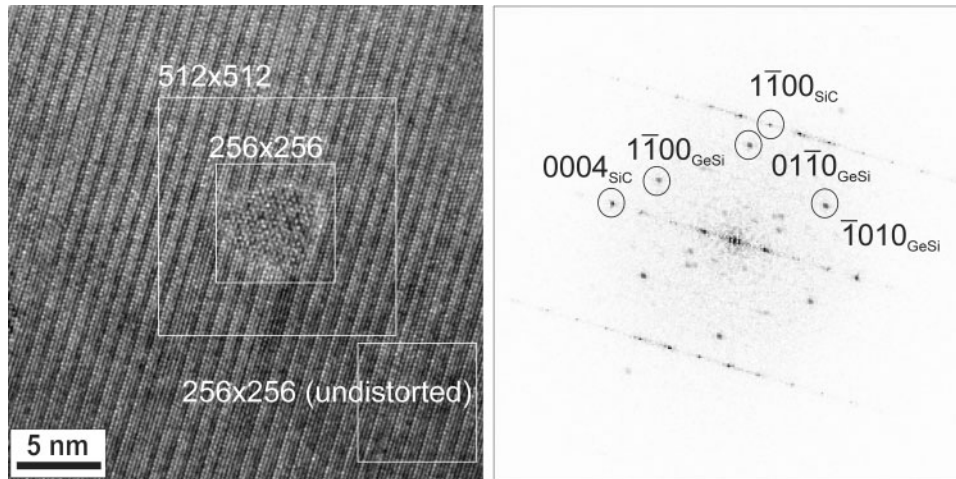
Fig. 7 The HRTEM image of a $Ge_{0.8}Si_{0.2}$ nanocrystal embedded in 6H-SiC (left). The parts of the image used for the lattice parameter determination are marked. The right figure shows a calculated diffractrogram. The reflections of the SiC are marked with a box. The measured reflections of the nanocrystal are encircled (see Table 2).

In order to obtain the highest accuracy, HRTEM images were recorded at $\times 400\,000$ magnification (see the section 'The influence of the diffraction vector length L^{-1}'). The whole HRTEM image (size 1024×1024 pixels) as well as the different parts of the image (512×512 and 256×256 pixels (Fig. 7)) were Fourier transformed. To determine the accuracy of the lattice parameters measurements for the matrix, first, an undistorted part of the defective 4H-SiC-image has been determined by comparing $d_{0004–4H-SiC,defective}$ and $d_{1-100–4H-SiC,defective}$ with $d_{0004–4H-SiC,perfect}$ and $d_{1-100–4H-SiC,perfect}$, respectively (see the part called 'undistorted' in Fig. 7). Second, the whole image and the parts of the image in the vicinity of the defect (Fig. 7) have been calibrated with the $d_{0004–4H-SiC,perfect}$. Afterwards, the values $d_{1-100–4H-SiC,defective}$ have been measured and

the strain value $(d - d_0)/d$ has been determined ($d = d_{1-100-4H-SiC,\ defective}, d_0 = d_{1-100-4H-SiC,\ perfect} = 0.2668$ nm). The values obtained are presented in the second row of Table 2, showing significant strain (limit of accuracy $\Delta d/d = 0.0002$) only for the image part in the direct vicinity of the defect. (The calculated strain in the whole image and in the undistorted part of the image is below the accuracy limit.).

To determine the accuracy of the lattice parameters measurements for the germanic silicon nanocrystal within the 4H-SiC matrix, a similar procedure has been applied. The *d*-values of the GeSi (encircled reflections 1, 2 and 3 in Fig. 7) have been measured and compared with the theoretical values ($d_{GeSi\ 1-100-} = 0.3436$ nm for $Ge_{0.8}Si_{0.2}$ [22]). The results are shown in Table2 (rows three to six). As seen for all reflections of the nanocrystals, significant strain has been
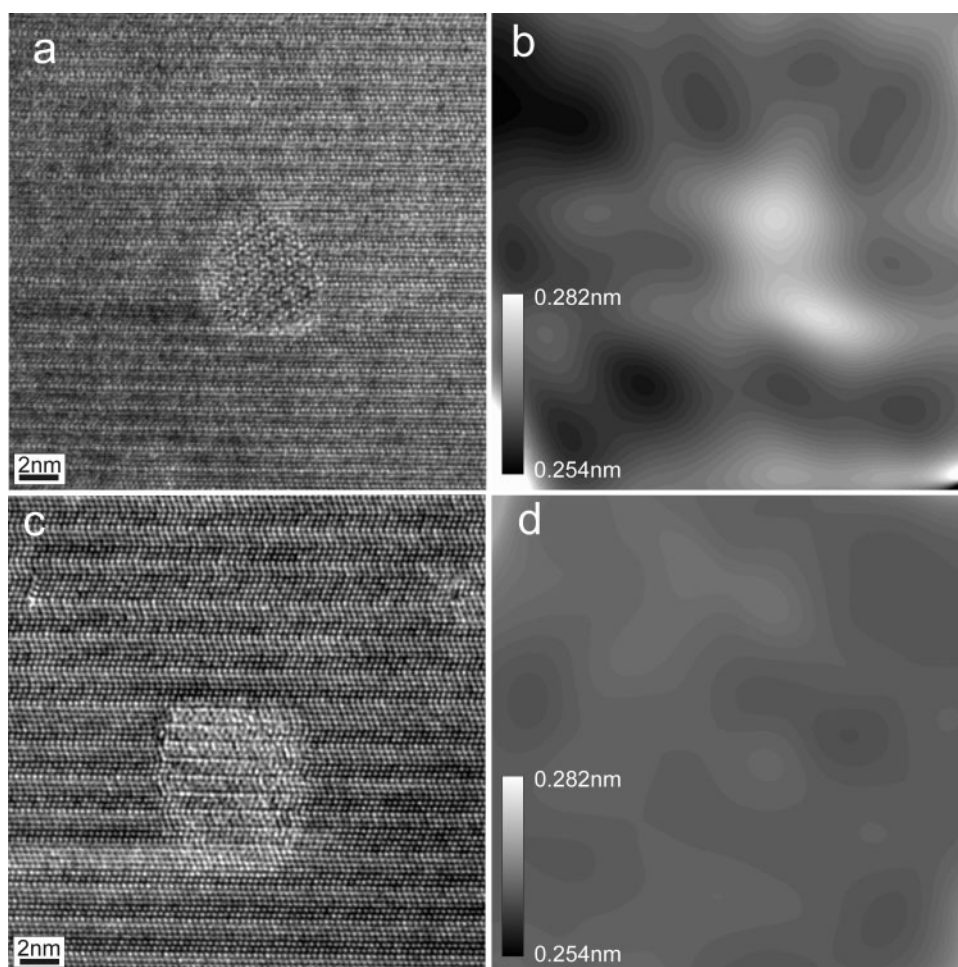
Fig. 8 The (11$\bar{2}$0) HRTEM images of embedded Ge$_{0.8}$Si$_{0.2}$ (a) and ErSi$_2$ (c) nanocrystals with the corresponding lattice bending maps for the 1$\bar{1}$00 reflection of the hexagonal SiC matrix (b, d). Note that the intensity bars in (b) and (d) are identical. The white regions at the outmost edges of the image are artifacts of the calculation method.

determined, which is visualized in the plot of lattice bending in Fig. 8b. Local changes of the vector length of $d_{1-100-4H\text{-}SiC}$ are plotted as different image intensities.

Figure 9 shows the d-values of the Ge nanocrystals as a function of L^{-1} obtained from the whole image and the different parts of the image in Fig. 7. The error bar Δd has been calculated using eq. (1). As can be seen, the smaller the image size, the larger Δd. Therefore, it can be concluded that the highest accuracy of the lattice parameters measurements of the nanocrystal can be obtained when the full image size instead of parts of the image are being examined. To verify the existence of strain, however, it is necessary to measure both the whole image and the smaller image parts, including the defect.

ErSi$_2$ nanocrystals embedded in 6H-SiC showed no significant deviation between $d_{1\text{-}100-6H\text{-}SiC,defective}$ and d$_{1\text{-}100-6H\text{-}SiC,perfect}$ ($d_0 = d_{1\text{-}100-6H\text{-}SiC,perfect} = 0.2668$ nm) (Table 3). Both nanocrystals and 6H-SiC matrix are unstrained (Table 3). This result obtained for the example shown in Fig. 8c is demonstrated in Fig. 8d. It can be seen
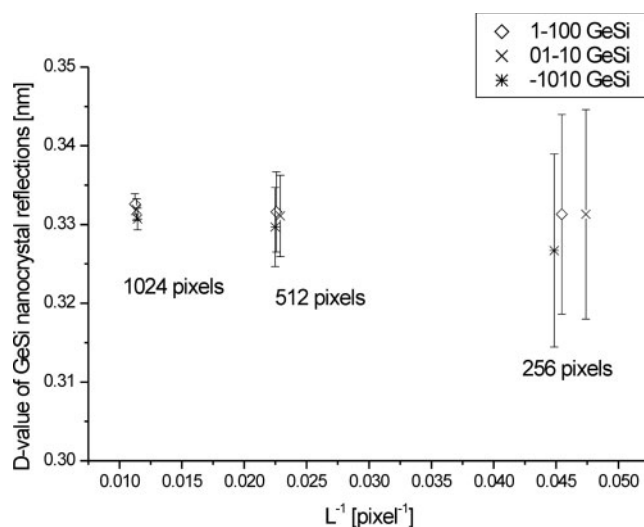
Fig. 9 The d-values of the Ge$_{0.8}$Si$_{0.2}$-nanocrystal reflections (compare with Fig. 7) as a function of L^{-1}. The error bars correspond to Δd, which was calculated using eq. (1).

Table 3. Measured *d*-values of the 6H-SiC matrix as well as the calculated strain for the different parts of the image shown in Fig. 9c. Table values are $d_{SiC1-100} = 0.2668$ nm. The strain has been calculated by $(d - d_0)/d$

	FFT box 1024 × 1024 (whole images)	FFT box 256 × 256 (around the nanocrystal)	FFT box 256 × 256 (undistorted area)
Measured value of 1$\bar{1}$00 (nm)	0.2666	0.2663	0.2671
Calculated strain	0.001	0.002	0.002

clearly that there are no significant changes of the image intensity (compared with Fig. 8b). The difference between GeSi and ErSi$_2$ nanocrystals has been attributed to the different chemical reaction during the creation of the nanocrystals [31].

Concluding remarks

In this study the accuracy ($\Delta d/d$) of the lattice parameter measurements from digitally recorded diffractograms has been evaluated for the case of perfect and for defective crystals.

For the case of a perfect crystal or a defective but unstrained crystal, two parameters have to be considered. These are the number of recorded lattice planes and the SNR of selected reflections. The accuracy was expressed by a linear function of the number of recorded lattice planes, which depends on the magnification and the *g*-vector length at a given magnification. To get the highest accuracy, we showed the following. First, the evaluated reflections should have the lowest possible *d*-value for the given magnification (longest *g*-vector in the reciprocal space analysis). Second, the recorded HRTEM image should be obtained at the lowest possible magnification. For the TEM and camera used and the plane spacings studied, advised magnifications are ×300 000–400 000. It has been shown that the SNR of reflections oscillated with the contrast transfer function (CTF). However, the accuracy of lattice parameters measurements stays unaffected for experimental conditions around Scherzer defocus. As the distortions of the microscope lenses become the limiting factor below $\Delta d/d = 0.002$ (0.0005 nm), for the TEM used, a better accuracy cannot be obtained.

The 2-D defects within the matrix do not change the limits of accuracy. For 3-D defects (embedded nanocrystals) we showed that it is the strain $((d-d_0)/d)$ which limits the accuracy of the measurement for both the nanocrystal and the matrix. This strain may therefore be treated as a systematic error that must be just added to the error of $\Delta d/d$ of the perfect crystal. Although a series of HRTEM images of a nanocrystal within a matrix may reduce the statistical error, for a quick estimation of the accuracy only the evaluation of a single HRTEM image is needed.

Acknowledgements

References

1 Bauer A, Kräusslich J, Dressler L, Kuschnerus, P, Wolf J, and Goetz K (1998) High-precision determination of atomic positions in crystals, case of 6h and 4h SIC. *Phys. Rev. B* **57:** 2647.

2 Krämer S, Mayer J, Witt C, Weickenmeier A, and Rühle M (2000) Analysis of local strain in Al interconnects by energy filtered CBED. *Ultramicroscopy* **81:** 245–262.

3 Kaiser U, Saitoh K, Tsuda K, and Tanaka M (1999) Application of the CBED method for the determination of lattice parameters of cubic SiC films on 6H-SiC substrates. *J. Electron Microsc.* **48:** 221–233.

4 Chuvilin A, Kups Th, and Kaiser U (2004) The effect of the signal-to-noise-ratio in CBED pattern on the accuracy of lattice parameter determination. *J. Electron Microsc.* **53:** 237–244.

5 Crozier P A, Tsen S C Y, Liu J, Lopez Cartes C, and Perez-Omil J A (1999) Factors affecting the accuracy of lattice spacing determination by HREM in nanometre-sized Pt particles. *J. Electron Microscopy* **48** [Suppl.]: 1015–1024.

6 Qin W and Fraundorf P (2003) Lattice parameters from direct-space images at two tilts. *Ultramicroscopy* **94:** 246.

7 de Ruijter W J (1994) Determination of lattice parameters from digital micrographs based on measurements in reciprocal space. *J. Comp. Assist. Microsc.* **6:** 130–134.

8 de Ruijter W J, Sharma R, McCartney M C, and Smith D J (1995) Measurement of lattice-fringe vectors from digital HREM images: experimental precision. *Ultramicroscopy* **57:** 409–422.

9 Rosenauer A, Kaiser S, Reisinger T, Zweck J, Gebhardt W, and Gerthsen D (1996) Digital analysis of high-resolution transmission electron microscopy lattice images. *Optik* **102:** 63–69.

10 Rosenauer A, Remmele T, Gerthsen D, Tillmann K, and Förster F (1997) Atomic scale strain measurements by the digital analysis of transmission electron microscope lattice fringes. *Optik* **105:** 99–107.

11 Hÿtch M J (1997) Analysis of variations in structure from high resolution electron microscope images by combining real space and Fourier space information. *Microsc. Microanal. Microstruct.* **8:** 41–57.

12 Hÿtch M J, Putaux J L, and Pénisson J M (2003) Measurement of the displacement field of dislocations to 0.03 Å by electron microscopy. *Nature* **423:** 270–273.

13 Dahmen U, Xiao S Q, Paciornik S, Johnson E, and Johansen A (1997) Magic-size equilibrium shapes of nanoscale Pb inclusions in Al. *Phys. Rev. Lett.* **78:** 471–474.

14 Tsen S C Y, Crozier P A, and Liu L (2003) Lattice measurement and alloy compositions in metal and bimetallic nanoparticles. *Ultramicroscopy* **98:** 63–72.

15 Malm J O and O'Keefe M A (1997) Deceptive 'lattice spacings' in high-resolution micrographs of metal nanoparticles. *Ultramicroscopy* **68:** 13–23.

16 Urban J (1998) Crystallography of clusters. *J. Cryst. Res. Technol.* **33:** 1009–1024.

17 Nihoul G, Sack-Kongehl H, and Urban J (1998) Electron microscopy structural characterisation of nano-materials: image simulation and image processing. *J. Cryst. Res. Technol.* **33:** 1024–1039.

18 Goyhenex C, Henry C R, and Urban J (1994) *In-situ* measurements of lattice parameters of supported palladium clusters. *Phil. Mag. A* **69:** 1073–1084.

19 Qin C and Peng L M (2002) Measurement accuracy of the diameter of a carbon nanotube from TEM images. *Phys. Rev. B* **65:** 155 431.

20 Schubert Ch, Kaiser U, Gorelik T, Hedler A, Kräusslich J, Wunderlich B, Hess G, Goetz K, Glatzel U, and Wesch W (2002) Formation of Ge nanocrystals in SiC by ion implantation and subsequent thermal annealing. *J. Appl. Phys*. **91:** 1520.

21 Kaiser U (2001) Nanocrystal formation in hexagonal SiC after Ge+ ion implantation. *J. Electron Microsc*. **50:** 251–263.

22 Kaiser U, Biskupek J, Muller D A, Gärtner K, and Schubert Ch (2002) Properties of GeSi nanocrystals embedded in hexagonal SiC. *J. Cryst. Res. Technol*. **37:** 391–406.

23 Kaiser U and Chuvilin A (2003) Enhanced compositional contrast in imaging of nanoprecipitates buried in a defective crystal using a conventional TEM. *Microsc. Microanal*. **9:** 36–41.

24 *Gatan Digital Micrograph User Manual*. (Gatan Inc., Pleasonton, CA.)

25 Hülk C (1998) *Charakterisierung von CCD-Kamerasystemen in der Transmissionselektronenmikroskopie und deren Einsatz bei der Erstellung von Elementverteilungsbildern*. (PhD Thesis, Mathematisch-Naturwissenschaftlichen Fakultät der Westfälischen Wilhelms-Universität Münster.).

26 Daberkow I and Hülk C (1998) Easy methods for accurate characterization of CCD cameras. *Proceedings of ICEM* **XIV:** 189.

27 Schoppies E (1988) *Halbleiter Elektronik*. (Bibliographisches Institut, Leipzig.)

28 Stadelmann P A (1987) EMS–a software package for electron diffraction analysis and HREM image simulation in material science. *Ultramicroscopy* **21:** 131–146.

29 Stadelmann P (2003) Image analysis and simulation software in transmission electron microscopy. *Microsc. Microanal*. **9** [Suppl.]: 60–61.

30 Reimer L (1993) *Transmission Electron Microscopy*. (Springer Verlag, Berlin.).

31 Kaiser U, Muller D A, Grazul J L, Chuvilin A, and Kawaskaki M (2000) Direct observation of defect-mediated cluster nucleation. *Nature Materials* **1–2:** 102–105.